periodogram[90] of each of those datasets. To represent the activity model we used a weighted average of the models for the different instruments. Figure 12 shows the best fit to the contemporary photometry and Figure 13 shows the best fit to the K2 observations.

## 3.1 Lessons learned and limitations.

We found that the signal phase-folded to the rotation period shows clearly the two modes of oscillation that our favoured GP Kernel describes. The amplitude of the rotation signal is 8 times larger than the amplitude measured for the signal related to V1298 Tau b, and 5 times larger than the signal related to planet e. In the context of young exoplanets, the stellar activity signals engulf those signals related to the planets and therefore similarly large observational efforts with precise RV measurements will be required.

We found that not all GP Kernels behaved the same at all timescales in our dataset. The classic QP Kernel handles short-period signals quite well. However for longer period signals it seems to absorb a significant part of the Keplerian components, causing a clear underestimation of the measured amplitudes. The mixture of SHO Kernels had the opposite behaviour. It *underfits* the activity component, leaving larger residuals and causing an overestimation of (some of) the Keplerian amplitudes. We found that our Kernel of choice (PQP2) provides better description of the activity variations of V1298 Tau and a more accurate determination of the Keplerian amplitudes.

It is important to remain cautious about the mass determined for the planet V1298 Tau e. The original detection did not constrain the orbital period, which is derived purely from the RV information. We studied the $S_{MW}$ index,[34] H$\alpha$ index,[35] NaI index[36] and TiO[37] chromospheric indicators following a very similar procedure as with the RV data, not finding any significant periodicity (aside from the rotation) at periods shorter than 150 days, which favours the planetary hypothesis. However, disentangling planetary signals from stellar activity in RV in young stars such as V1298 Tau is a very challenging task. Without the confirmation of its orbital period by transit photometry it is very difficult to completely exclude a stellar origin (or contribution) to the signal.

# References


[1] Mordasini, C. *et al.* Characterization of exoplanets from their formation. II. The planetary mass-radius relationship. *Astron. Astrophys.* **547**, A112 (2012).

[2] D'Angelo, G., Weidenschilling, S. J., Lissauer, J. J. & Bodenheimer, P. Growth of Jupiter: Formation in disks of gas and solids and evolution to the present epoch. *Icarus* **355**, 114087 (2021).

[3] Donati, J. F. *et al.* A hot Jupiter orbiting a 2-million-year-old solar-mass T Tauri star. *Nature* **534**, 662–666 (2016).

[4] Damasso, M. *et al.* The GAPS Programme at TNG. XXVII. Reassessment of a young planetary system with HARPS-N: is the hot Jupiter V830 Tau b really there? *Astron. Astrophys.* **642**, A133 (2020).

[5] David, T. J., Hillenbrand, L. A., Cody, A. M., Carpenter, J. M. & Howard, A. W. K2 Discovery of Young Eclipsing Binaries in Upper Scorpius: Direct Mass and Radius Determinations for the Lowest Mass Stars and Initial Characterization of an Eclipsing Brown Dwarf Binary. *Astrophys. J.* **816**, 21 (2016).

[6] Plavchan, P. *et al.* A planet within the debris disk around the pre-main-sequence star AU Microscopii. *Nature* **582**, 497–500 (2020).

[7] Klein, B. *et al.* Investigating the young AU Mic system with SPIRou: large-scale stellar magnetic field and close-in planet mass. *Mon. Not. R. Astron. Soc.* **502**, 188–205 (2021).

[8] David, T. J. *et al.* A Warm Jupiter-sized Planet Transiting the Pre-main-sequence Star V1298 Tau. *Astron. J.* **158**, 79 (2019).

[9] David, T. J. *et al.* Four Newborn Planets Transiting the Young Solar Analog V1298 Tau. *Astrophys. J. Lett.* **885**, L12 (2019).

[10] Brahm, R. *et al.* HATS-17b: A Transiting Compact Warm Jupiter in a 16.3 Day Circular Orbit. *Astron. J.* **151**, 89 (2016).

[11] Mancini, L. *et al.* Kepler-539: A young extrasolar system with two giant planets on wide orbits and in gravitational interaction. *Astron. Astrophys.* **590**, A112 (2016).

[12] Oh, S., Price-Whelan, A. M., Hogg, D. W., Morton, T. D. & Spergel, D. N. Comoving Stars in Gaia DR1: An Abundance of Very Wide Separation Comoving Pairs. *Astron. J.* **153**, 257 (2017).

[13] Howell, S. B. *et al.* The K2 Mission: Characterization and Early Results. *Publ. Astron. Soc. Pac.* **126**, 398 (2014).

[14] Beichman, C. *et al.* A Mass Limit for the Young Transiting Planet V1298 Tau b. *Research Notes of the American Astronomical Society* **3**, 89 (2019).

[15] Brown, T. M. *et al.* Las Cumbres Observatory Global Telescope Network. *Publ. Astron. Soc. Pac.* **125**, 1031 (2013).

[16] Rasmussen, C. E. & Williams, C. K. I. *Gaussian Processes for Machine Learning* (2006).

[17] David, T. J. *et al.* Age Determination in Upper Scorpius with Eclipsing Binaries. *Astrophys. J.* **872**, 161 (2019).

[18] Fortney, J. J., Marley, M. S. & Barnes, J. W. Planetary Radii across Five Orders of Magnitude in Mass and Stellar Insolation: Application to Transits. *Astrophys. J.* **659**, 1661–1672 (2007).

[19] Baraffe, I., Chabrier, G. & Barman, T. Structure and evolution of super-Earth to super-Jupiter exoplanets. I. Heavy element enrichment in the interior. *Astron. Astrophys.* **482**, 315–332 (2008).

[20] Emsenhuber, A. *et al.* The New Generation Planetary Population Synthesis (NGPPS). II. Planetary population of solar-like stars and overview of statistical results. *arXiv e-prints* arXiv:2007.05562 (2020).

[21] Poppenhaeger, K., Ketzer, L. & Mallonn, M. X-ray irradiation and evaporation of the four young planets around V1298 Tau. *Mon. Not. R. Astron. Soc.* **500**, 4560–4572 (2021).

[22] Thorngren, D. P., Fortney, J. J., Murray-Clay, R. A. & Lopez, E. D. The Mass-Metallicity Relation for Giant Planets. *Astrophys. J.* **831**, 64 (2016).

[23] Wahl, S. M. *et al.* Comparing Jupiter interior structure models to Juno gravity measurements and the role of a dilute core. *Geophys. Res. Lett.* **44**, 4649–4659 (2017).

[24] Turrini, D. *et al.* Tracing the Formation History of Giant Planets in Protoplanetary Disks with Carbon, Oxygen, Nitrogen, and Sulfur. *Astrophys. J.* **909**, 40 (2021).

[25] Gaia Collaboration *et al.* Gaia Early Data Release 3. Summary of the contents and survey properties. *Astron. Astrophys.* **649**, A1 (2021).

[26] Gaia Collaboration *et al.* Gaia Data Release 2. Summary of the contents and survey properties. *Astron. Astrophys.* **616**, A1 (2018).

[27] Nguyen, D. C., Brandeker, A., van Kerkwijk, M. H. & Jayawardhana, R. Close Companions to Young Stars. I. A Large Spectroscopic Survey in Chamaeleon I and Taurus-Auriga. *Astrophys. J.* **745**, 119 (2012).

[28] Nesterov, V. V. *et al.* The Henry Draper Extension Charts: A catalogue of accurate positions, proper motions, magnitudes and spectral types of 86933 stars. *Astron. Astrophys. Suppl.* **110**, 367 (1995).

[29] Høg, E. *et al.* The Tycho-2 catalogue of the 2.5 million brightest stars. *Astron. Astrophys.* **355**, L27–L30 (2000).

[30] Skrutskie, M. F. *et al.* The Two Micron All Sky Survey (2MASS). *Astron. J.* **131**, 1163–1183 (2006).

[31] Cosentino, R. *et al.* Harps-N: the new planet hunter at TNG. In McLean, I. S., Ramsay, S. K. & Takami, H. (eds.) *Ground-based and Airborne Instrumentation for Astronomy IV*,

vol. 8446 of *Society of Photo-Optical Instrumentation Engineers (SPIE) Conference Series*, 84461V (2012).

[32] Covino, E. *et al.* The GAPS programme with HARPS-N at TNG. I. Observations of the Rossiter-McLaughlin effect and characterisation of the transiting system Qatar-1. *Astron. Astrophys.* **554**, A28 (2013).

[33] Carleo, I. *et al.* The GAPS Programme at TNG. XXI. A GIARPS case study of known young planetary candidates: confirmation of HD 285507 b and refutation of AD Leonis b. *Astron. Astrophys.* **638**, A5 (2020).

[34] Noyes, R. W., Hartmann, L. W., Baliunas, S. L., Duncan, D. K. & Vaughan, A. H. Rotation, convection, and magnetic activity in lower main-sequence stars. *ApJ* **279**, 763–777 (1984).

[35] Gomes da Silva, J. *et al.* Long-term magnetic activity of a sample of M-dwarf stars from the HARPS program. I. Comparison of activity indices. *A&A* **534**, A30 (2011).

[36] Díaz, R. F., Cincunegui, C. & Mauas, P. J. D. The NaI D resonance lines in main-sequence late-type stars. *Mon. Not. R. Astron. Soc.* **378**, 1007–1018 (2007).

[37] Azizi, F. & Mirtorabi, M. T. A survey of TiO$\lambda$567 nm absorption in solar-type stars. *Mon. Not. R. Astron. Soc.* **475**, 2253–2268 (2018).

[38] Quirrenbach, A. *et al.* CARMENES instrument overview. In Ramsay, S. K., McLean, I. S. & Takami, H. (eds.) *Ground-based and Airborne Instrumentation for Astronomy V*, vol. 9147 of *Society of Photo-Optical Instrumentation Engineers (SPIE) Conference Series*, 91471F (2014).

[39] Zechmeister, M., Anglada-Escudé, G. & Reiners, A. Flat-relative optimal extraction. A quick and efficient algorithm for stabilised spectrographs. *Astron. Astrophys.* **561**, A59 (2014).

[40] Raskin, G. *et al.* HERMES: a high-resolution fibre-fed spectrograph for the Mercator telescope. *Astron. Astrophys.* **526**, A69 (2011).

[41] Baranne, A. *et al.* ELODIE: A spectrograph for accurate radial velocity measurements. *Astron. Astrophys. Suppl.* **119**, 373–390 (1996).

[42] Strassmeier, K. G. *et al.* The STELLA robotic observatory. *Astronomische Nachrichten* **325**, 527–532 (2004).

[43] Collins, K. A., Kielkopf, J. F., Stassun, K. G. & Hessman, F. V. AstroImageJ: Image Processing and Photometric Extraction for Ultra-precise Astronomical Light Curves. *Astron. J.* **153**, 77 (2017).

[44] Luger, R., Kruse, E., Foreman-Mackey, D., Agol, E. & Saunders, N. An Update to the EVEREST K2 Pipeline: Short Cadence, Saturated Stars, and Kepler-like Photometry Down to Kp = 15. *Astron. J.* **156**, 99 (2018).

[45] Deming, D. *et al.* Infrared Transmission Spectroscopy of the Exoplanets HD 209458b and XO-1b Using the Wide Field Camera-3 on the Hubble Space Telescope. *Astrophys. J.* **774**, 95 (2013).

[46] Luhman, K. L. The Stellar Membership of the Taurus Star-forming Region. *Astron. J.* **156**, 271 (2018).

[47] Andrews, J. J., Chanamé, J. & Agüeros, M. A. Wide binaries in Tycho-Gaia: search method and the distribution of orbital separations. *Mon. Not. R. Astron. Soc.* **472**, 675–699 (2017).

[48] González Hernández, J. I. *et al.* The solar gravitational redshift from HARPS-LFC Moon spectra⋆. A test of the general theory of relativity. *Astron. Astrophys.* **643**, A146 (2020).

[49] Suárez Mascareño, A. *et al.* The RoPES project with HARPS and HARPS-N. I. A system of super-Earths orbiting the moderately active K-dwarf HD 176986. *Astron. Astrophys.* **612**, A41 (2018).

[50] Foreman-Mackey, D., Hogg, D. W., Lang, D. & Goodman, J. emcee: The MCMC Hammer. *Publ. Astron. Soc. Pac.* **125**, 306 (2013).

[51] Allende Prieto, C. *et al.* A Spectroscopic Study of the Ancient Milky Way: F- and G-Type Stars in the Third Data Release of the Sloan Digital Sky Survey. *Astrophys. J.* **636**, 804–820 (2006).

[52] Allende Prieto, C. *et al.* A collection of model stellar spectra for spectral types B to early-M. *Astron. Astrophys.* **618**, A25 (2018).

[53] Asplund, M., Grevesse, N., Sauval, A. J. & Scott, P. The Chemical Composition of the Sun. *Annu. Rev. Astron. Astrophys.* **47**, 481–522 (2009).

[54] Kurucz, R. L., Furenlid, I., Brault, J. & Testerman, L. *Solar flux atlas from 296 to 1300 nm* (1984).

[55] Dutra-Ferreira, L., Pasquini, L., Smiljanic, R., Porto de Mello, G. F. & Steffen, M. Consistent metallicity scale for cool dwarfs and giants. A benchmark test using the Hyades. *Astron. Astrophys.* **585**, A75 (2016).

[56] Castelli, F. & Kurucz, R. L. New Grids of ATLAS9 Model Atmospheres. In Piskunov, N., Weiss, W. W. & Gray, D. F. (eds.) *Modelling of Stellar Atmospheres*, vol. 210, A20 (2003).

[57] González Hernández, J. I. & Bonifacio, P. A new implementation of the infrared flux method using the 2MASS catalogue. *Astron. Astrophys.* **497**, 497–509 (2009).

[58] Henden, A. A., Levine, S. E., Terrell, D., Smith, T. C. & Welch, D. Data Release 3 of the AAVSO All-Sky Photometric Survey (APASS). *Journal of the American Association of Variable Star Observers (JAAVSO)* **40**, 430 (2012).

[59] Schlegel, D. J., Finkbeiner, D. P. & Davis, M. Maps of Dust Infrared Emission for Use in Estimation of Reddening and Cosmic Microwave Background Radiation Foregrounds. *Astrophys. J.* **500**, 525–553 (1998).

[60] Bonifacio, P., Monai, S. & Beers, T. C. A Search for Stars of Very Low Metal Abundance. V. Photoelectric UBV Photometry of Metal-weak Candidates from the Northern HK Survey. *Astron. J.* **120**, 2065–2081 (2000).

[61] Sneden, C. A. *Carbon and Nitrogen Abundances in Metal-Poor Stars.* Ph.D. thesis, THE UNIVERSITY OF TEXAS AT AUSTIN. (1973).

[62] Lind, K., Asplund, M. & Barklem, P. S. Departures from LTE for neutral Li in late-type stars. *Astron. Astrophys.* **503**, 541–544 (2009).

[63] Peacock, M. B., Zepf, S. E. & Finzell, T. Signatures of Multiple Stellar Populations in Unresolved Extragalactic Globular/Young Massive Star Clusters. *Astrophys. J.* **769**, 126 (2013).

[64] Bayo, A. *et al.* VOSA: virtual observatory SED analyzer. An application to the Collinder 69 open cluster. *Astron. Astrophys.* **492**, 277–287 (2008).

[65] Baraffe, I., Homeier, D., Allard, F. & Chabrier, G. New evolutionary models for pre-main sequence and main sequence low-mass stars down to the hydrogen-burning limit. *Astron. Astrophys.* **577**, A42 (2015).

[66] Tognelli, E., Prada Moroni, P. G. & Degl'Innocenti, S. The Pisa pre-main sequence tracks and isochrones. A database covering a wide range of Z, Y, mass, and age values. *Astron. Astrophys.* **533**, A109 (2011).

[67] Bressan, A. *et al.* PARSEC: stellar tracks and isochrones with the PAdova and TRieste Stellar Evolution Code. *Mon. Not. R. Astron. Soc.* **427**, 127–145 (2012).

[68] del Burgo, C. & Allende Prieto, C. Testing models of stellar structure and evolution - I. Comparison with detached eclipsing binaries. *Mon. Not. R. Astron. Soc.* **479**, 1953–1973 (2018).

[69] Miret-Roig, N. *et al.* Dynamical traceback age of the $\beta$ Pictoris moving group. *arXiv e-prints* arXiv:2007.10997 (2020).

[70] Rebull, L. M. *et al.* Rotation of Low-mass Stars in Taurus with K2. *Astron. J.* **159**, 273 (2020).

[71] Dahm, S. E. Reexamining the Lithium Depletion Boundary in the Pleiades and the Inferred Age of the Cluster. *Astrophys. J.* **813**, 108 (2015).

[72] Gossage, S. *et al.* Age Determinations of the Hyades, Praesepe, and Pleiades via MESA Models with Rotation. *Astrophys. J.* **863**, 67 (2018).

[73] Gutiérrez Albarrán, M. L. *et al.* The Gaia-ESO Survey: Calibrating the lithium-age relation with open clusters and associations. I. Cluster age range and initial membership selections. *arXiv e-prints* arXiv:2009.00610 (2020).

[74] Barrado y Navascués, D., Stauffer, J. R. & Patten, B. M. The Lithium-Depletion Boundary and the Age of the Young Open Cluster IC 2391. *Astrophys. J. Lett.* **522**, L53–L56 (1999).

[75] Wichmann, R. *et al.* New weak-line T Tauri stars in Taurus-Auriga. *Astron. Astrophys.* **312**, 439–454 (1996).

[76] Micela, G. *et al.* Deep ROSAT HRI observations of the Pleiades. *Astron. Astrophys.* **341**, 751–767 (1999).

[77] Fang, X.-S., Zhao, G., Zhao, J.-K. & Bharat Kumar, Y. Stellar activity with LAMOST - II. Chromospheric activity in open clusters. *Mon. Not. R. Astron. Soc.* **476**, 908–926 (2018).

[78] Findeisen, K., Hillenbrand, L. & Soderblom, D. Stellar Activity in the Broadband Ultraviolet. *Astron. J.* **142**, 23 (2011).

[79] Foreman-Mackey, D., Agol, E., Ambikasaran, S. & Angus, R. Fast and Scalable Gaussian Process Modeling with Applications to Astronomical Time Series. *Astron. J.* **154**, 220 (2017).

[80] Haywood, R. D. *et al.* Planets and stellar activity: hide and seek in the CoRoT-7 system. *MNRAS* **443**, 2517–2531 (2014).

[81] Suárez Mascareño, A. *et al.* Revisiting Proxima with ESPRESSO. *Astron. Astrophys.* **639**, A77 (2020).

[82] Parviainen, H. PYTRANSIT: fast and easy exoplanet transit modelling in PYTHON. *Mon. Not. R. Astron. Soc.* **450**, 3233–3238 (2015).

[83] Mandel, K. & Agol, E. Analytic Light Curves for Planetary Transit Searches. *Astrophys. J. Lett.* **580**, L171–L175 (2002).

[84] Fulton, B. J., Petigura, E. A., Blunt, S. & Sinukoff, E. RadVel: The Radial Velocity Modeling Toolkit. *Publ. Astron. Soc. Pac.* **130**, 044504 (2018).

[85] Skilling, J. Nested Sampling. In Fischer, R., Preuss, R. & Toussaint, U. V. (eds.) *Bayesian Inference and Maximum Entropy Methods in Science and Engineering: 24th International Workshop on Bayesian Inference and Maximum Entropy Methods in Science and Engineering*, vol. 735 of *American Institute of Physics Conference Series*, 395–405 (2004).

[86] Speagle, J. S. DYNESTY: a dynamic nested sampling package for estimating Bayesian posteriors and evidences. *Mon. Not. R. Astron. Soc.* **493**, 3132–3158 (2020).

[87] Ambikasaran, S., Foreman-Mackey, D., Greengard, L., Hogg, D. W. & O'Neil, M. Fast Direct Methods for Gaussian Processes. *IEEE Transactions on Pattern Analysis and Machine Intelligence* **38**, 252 (2015).

[88] Benatti, S. *et al.* Constraints on the mass and atmospheric composition and evolution of the low-density young planet DS Tuc A b. *arXiv e-prints* arXiv:2103.12922 (2021).

[89] Feng, F., Tuomi, M., Jones, H. R. A., Butler, R. P. & Vogt, S. A Goldilocks principle for modelling radial velocity noise. *Mon. Not. R. Astron. Soc.* **461**, 2440–2452 (2016).

[90] Zechmeister, M. & Kürster, M. The generalised Lomb-Scargle periodogram. A new formalism for the floating-mean and Keplerian periodograms. *Astron. Astrophys.* **496**, 577–584 (2009).

**Code availability** The `SERVAL` template-matching radial velocity measurement tool, `Celerite`, `George`, `EMCEE`, `dynesty`, `RADVEL`, `PyTransit`, `AstroImageJ`, `SYNPLE`,`StePar`, `FERRE` and `MOOG` are easily accessible open source projects. Additional software available upon request.

**Data availability** The public high-resolution spectroscopic raw data used in the study can be freely downloaded from the corresponding facility archives. Proprietary raw data are available from A.S.M on reasonable request.

Table 3: Parameters and priors for the combined model. The column "Dataset" shows between which datasets the parameter is shared during the optimisation. All T0*s* are expressed in BJD - 2450000. Datasets: 1 - K2; 2 - LCO; 3 - HARPS-N RV; 4 - CARMENES RV; 5 - SES RV; 6 - HERMES RV. [1]The correlation model ( 4p $_{Corr}$) uses a different amount of data.

| **Parameter** | **Dataset** | **Priors** | **4p** $_{PQP2}$ | **4p** $_{Damped}$ | **4p** $_{QP}$ | **4p** $_{Corr}$ |
|---|---|---|---|---|---|---|
| *Planets* | | | | | | |
| T0 b [d] | 1,3,4,5,6 | $\mathcal{N}$ (7067.0488, 0.25) | $7067.0486^{+0.0015}_{-0.0016}$ | $7067.0485^{+0.0016}_{-0.0017}$ | $7067.0488^{+0.0016}_{-0.0017}$ | $7067.0484^{+0.0032}_{-0.0038}$ |
| P b [d] | 1,3,4,5,6 | $\mathcal{N}$ (24.1396, 0.25) | $24.1399^{+0.0016}_{-0.0015}$ | $24.14^{+0.0016}_{-0.0016}$ | $24.1396^{+0.0016}_{-0.0016}$ | $24.14^{+0.0034}_{-0.0031}$ |
| $R_p/R_*$ b | 1 | $\mathcal{U}$ (0 , 0.2) | $0.0698^{+0.0024}_{-0.0023}$ | $0.0711^{+0.0029}_{-0.0029}$ | $0.0715^{+0.0024}_{-0.0024}$ | $0.0695^{+0.0037}_{-0.0038}$ |
| Imp b | 1 | $\mathcal{U}$ (0 , 1) | $0.33^{+0.12}_{-0.14}$ | $0.45^{+0.08}_{-0.16}$ | $0.45^{+0.06}_{-0.08}$ | $0.32^{+0.1}_{-0.15}$ |
| K b [m·s$^{-1}$] | 3,4,5,6 | $\mathcal{U}$ (0 , 200) | $41^{+12}_{-12}$ | $54.6^{+7.6}_{-7.8}$ | $31^{+18}_{-17}$ | $57^{+20}_{-20}$ |
| $\sqrt{e}\cdot\cos\omega$ b | 1,3,4,5,6 | $\mathcal{U}$ (0 , 0.5) | $0.31^{+0.12}_{-0.16}$ | $0.35^{+0.07}_{-0.09}$ | $0.02^{+0.22}_{-0.22}$ | $0.05^{+0.23}_{-0.22}$ |
| $\sqrt{e}\cdot\sin\omega$ b | 1,3,4,5,6 | $\mathcal{U}$ (0 , 0.5) | $-0.06^{+0.14}_{-0.17}$ | $-0.09^{+0.19}_{-0.17}$ | $-0.0^{+0.17}_{-0.2}$ | $-0.01^{+0.16}_{-0.18}$ |
| T0 c [d] | 1,3,4,5,6 | $\mathcal{N}$ (7064.2797, 0.25) | $7064.2801^{+0.0039}_{-0.0046}$ | $7064.2806^{+0.0037}_{-0.0042}$ | $7064.2785^{+0.0045}_{-0.005}$ | $7064.2778^{+0.0081}_{-0.0084}$ |
| P c [d] | 1,3,4,5,6 | $\mathcal{N}$ (8.24958, 0.25) | $8.2492^{+0.001}_{-0.0008}$ | $8.249^{+0.00094}_{-0.00081}$ | $8.2508^{+0.0014}_{-0.0013}$ | $8.2498^{+0.0018}_{-0.0016}$ |
| $R_p/R_*$ c | 1 | $\mathcal{U}$ (0 , 0.2) | $0.0371^{+0.0019}_{-0.0019}$ | $0.0372^{+0.0017}_{-0.0017}$ | $0.0368^{+0.002}_{-0.002}$ | $0.0361^{+0.0031}_{-0.0035}$ |
| Imp c | 1 | $\mathcal{U}$ (0 , 1) | $0.26^{+0.13}_{-0.15}$ | $0.25^{+0.14}_{-0.15}$ | $0.22^{+0.15}_{-0.14}$ | $0.17^{+0.16}_{-0.11}$ |
| K c [m·s$^{-1}$] | 3,4,5,6 | $\mathcal{U}$ (0 , 200) | $4.0^{+4.9}_{-2.9}$ | $3.6^{+4.3}_{-2.6}$ | $10.1^{+4.0}_{-4.2}$ | $14.3^{+12.9}_{-9.7}$ |
| $\sqrt{e}\cdot\cos\omega$ c | 1,3,4,5,6 | $\mathcal{U}$ (0 , 0.5) | $-0.03^{+0.26}_{-0.22}$ | $0.01^{+0.25}_{-0.24}$ | $0.32^{+0.12}_{-0.2}$ | $-0.03^{+0.18}_{-0.2}$ |
| $\sqrt{e}\cdot\sin\omega$ c | 1,3,4,5,6 | $\mathcal{U}$ (0 , 0.5) | $-0.24^{+0.12}_{-0.12}$ | $-0.11^{+0.16}_{-0.16}$ | $-0.15^{+0.11}_{-0.12}$ | $-0.15^{+0.18}_{-0.13}$ |
| T0 d [d] | 1,3,4,5,6 | $\mathcal{N}$ (7072.3913, 0.25) | $7072.3907^{+0.0063}_{-0.0045}$ | $7072.3902^{+0.0038}_{-0.0033}$ | $7072.3956^{+0.0053}_{-0.0058}$ | $7072.3903^{+0.0071}_{-0.0061}$ |
| P d [d] | 1,3,4,5,6 | $\mathcal{N}$ (12.4032, 0.25) | $12.4054^{+0.0018}_{-0.0017}$ | $12.4053^{+0.0019}_{-0.0017}$ | $12.4047^{+0.003}_{-0.0019}$ | $12.4058^{+0.0027}_{-0.0026}$ |
| $R_p/R_*$ d | 1 | $\mathcal{U}$ (0 , 0.2) | $0.0462^{+0.0021}_{-0.0021}$ | $0.0464^{+0.002}_{-0.0021}$ | $0.0459^{+0.0024}_{-0.0025}$ | $0.046^{+0.0037}_{-0.004}$ |
| Imp d | 1 | $\mathcal{U}$ (0 , 1) | $0.12^{+0.11}_{-0.08}$ | $0.18^{+0.14}_{-0.12}$ | $0.21^{+0.15}_{-0.14}$ | $0.19^{+0.13}_{-0.12}$ |
| K d [m·s$^{-1}$] | 3,4,5,6 | $\mathcal{U}$ (0 , 200) | $5.2^{+5.9}_{-3.7}$ | $2.2^{+3.0}_{-1.6}$ | $4.6^{+4.3}_{-3.1}$ | $7.0^{+9.2}_{-5.0}$ |
| $\sqrt{e}\cdot\cos\omega$ d | 1,3,4,5,6 | $\mathcal{N}$ (0 , 0.5) | $-0.01^{+0.16}_{-0.16}$ | $-0.03^{+0.23}_{-0.21}$ | $0.03^{+0.17}_{-0.2}$ | $-0.04^{+0.2}_{-0.19}$ |
| $\sqrt{e}\cdot\sin\omega$ d | 1,3,4,5,6 | $\mathcal{N}$ (0 , 0.5) | $-0.1^{+0.13}_{-0.14}$ | $-0.06^{+0.16}_{-0.13}$ | $0.04^{+0.14}_{-0.15}$ | $-0.17^{+0.15}_{-0.11}$ |
| T0 e [d] | 1,3,4,5,6 | $\mathcal{N}$ (7096.6229, 0.25) | $7096.6227^{+0.0033}_{-0.0032}$ | $7096.6227^{+0.0032}_{-0.003}$ | $7097.1913^{+0.0018}_{-0.0036}$ | $7096.6234^{+0.0089}_{-0.0083}$ |

*Continued on next page*

Table 3 – *Continued from previous page*

| | | | | | | |
|---|---|---|---|---|---|---|
| Ln P e [d] | 1,3,4,5,6 | $\mathcal{U}$ (Ln(35),Ln(400)) | $3.693^{+0.023}_{-0.023}$ | $3.65^{+0.043}_{-0.022}$ | $3.718^{+0.049}_{-0.026}$ | $3.717^{+0.048}_{-0.046}$ |
| $R_p/R_*$ e | 1 | $\mathcal{U}$ (0 , 0.2) | $0.0592^{+0.0046}_{-0.0048}$ | $0.0599^{+0.0045}_{-0.0047}$ | $0.0695^{+0.0045}_{-0.0048}$ | $0.0542^{+0.0096}_{-0.0131}$ |
| Imp e | 1 | $\mathcal{U}$ (0 , 1) | $0.41^{+0.1}_{-0.15}$ | $0.45^{+0.08}_{-0.15}$ | $0.52^{+0.09}_{-0.13}$ | $0.4^{+0.16}_{-0.21}$ |
| K e [m·s$^{-1}$] | 3,4,5,6 | $\mathcal{U}$ (0 , 200) | $62^{+15}_{-16}$ | $59.4^{+7.8}_{-7.7}$ | $36^{+13}_{-14}$ | $80^{+20}_{-20}$ |
| $\sqrt{e}\cdot\cos\omega$ e | 1,3,4,5,6 | $\mathcal{U}$ (0 , 0.5) | $0.22^{+0.18}_{-0.25}$ | $0.21^{+0.16}_{-0.23}$ | $-0.02^{+0.32}_{-0.26}$ | $0.16^{+0.2}_{-0.26}$ |
| $\sqrt{e}\cdot\sin\omega$ e | 1,3,4,5,6 | $\mathcal{U}$ (0 , 0.5) | $-0.03^{+0.2}_{-0.2}$ | $0.04^{+0.2}_{-0.22}$ | $0.27^{+0.13}_{-0.26}$ | $0.04^{+0.19}_{-0.24}$ |
| *Activity* | | | | | | |
| Ln A [ppt] | 1 | $\mathcal{U}$ (-10 , 10) | $2.71^{+0.27}_{-0.25}$ | $2.85^{+0.33}_{-0.3}$ | $2.95^{+0.64}_{-0.46}$ | $3.16^{+0.93}_{-0.68}$ |
| Ln A [ppt] | 2 | $\mathcal{U}$ (-10 , 10) | $3.27^{+0.2}_{-0.17}$ | $3.32^{+0.23}_{-0.28}$ | $3.45^{+0.23}_{-0.2}$ | |
| Ln A RV [m·s$^{-1}$] | 3 | $\mathcal{U}$ (-10 , 10) | $5.53^{+0.19}_{-0.17}$ | $5.28^{+0.19}_{-0.18}$ | $5.44^{+0.12}_{-0.11}$ | $-3.25^{+4.21}_{-4.49}$ |
| Ln A RV [m·s$^{-1}$] | 4 | $\mathcal{U}$ (-10 , 10) | $5.54^{+0.22}_{-0.2}$ | $5.33^{+0.26}_{-0.39}$ | $5.46^{+0.16}_{-0.15}$ | $-3.1^{+4.15}_{-3.94}$ |
| Ln A RV [m·s$^{-1}$] | 5 | $\mathcal{U}$ (-10 , 10) | $5.58^{+0.23}_{-0.22}$ | $5.21^{+0.24}_{-0.22}$ | $5.65^{+0.16}_{-0.16}$ | $-3.05^{+4.74}_{-4.23}$ |
| Ln A RV [m·s$^{-1}$] | 6 | $\mathcal{U}$ (-10 , 10) | $6.01^{+0.25}_{-0.26}$ | $5.68^{+0.26}_{-0.23}$ | $5.98^{+0.19}_{-0.17}$ | $-3.96^{+4.86}_{-4.09}$ |
| $P_{rot}$ 2015 [d] | 1 | $\mathcal{U}$ (2.75 , 3.1) | $2.868^{+0.013}_{-0.013}$ | $2.868^{+0.013}_{-0.012}$ | $2.867^{+0.013}_{-0.012}$ | $2.871^{+0.027}_{-0.026}$ |
| Ln $T_{Scale\ 1}$ 2015 [d] | 1 | $\mathcal{U}$ (-10 , 10) | $5.41^{+0.69}_{-0.67}$ | $5.7^{+0.76}_{-0.76}$ | $6.04^{+1.33}_{-1.03}$ | $6.09^{+1.88}_{-1.93}$ |
| Ln $T_{Scale\ 2}$ 2015 [d] | 1 | $\mathcal{U}$ (-10 , 10) | $0.75^{+0.21}_{-0.18}$ | $0.73^{+0.19}_{-0.16}$ | $0.64^{+0.2}_{-0.17}$ | $0.83^{+0.58}_{-0.33}$ |
| $P_{rot}$ 2019 [d] | 2,3,4,5,6 | $\mathcal{U}$ (2.75 , 3.1) | $2.9101^{+0.002}_{-0.002}$ | $2.9103^{+0.0019}_{-0.0017}$ | $2.9001^{+0.0028}_{-0.0028}$ | $2.887^{+0.1534}_{-0.1646}$ |
| Ln $T_{Scale\ 1}$ 2019 [d] | 2,3,4,5,6 | $\mathcal{U}$ (-10 , 10) | $5.34^{+0.4}_{-0.35}$ | $4.05^{+0.85}_{-0.47}$ | $3.26^{+0.08}_{-0.09}$ | |
| Ln $T_{Scale\ 2}$ 2019 [d] | 2,3,4,5,6 | $\mathcal{U}$ (-10 , 10) | $4.98^{+0.45}_{-0.4}$ | $5.91^{+0.64}_{-0.59}$ | | |
| Ln Mix RV | 3,4,5,6 | $\mathcal{U}$ (-10 , 10) | $-0.19^{+0.21}_{-0.21}$ | $-0.12^{+0.25}_{-0.23}$ | | |
| Ln Mix Phot | 1,2 | $\mathcal{U}$ (-10 , 10) | $-0.91^{+0.24}_{-0.27}$ | $-1.06^{+0.3}_{-0.33}$ | $-1.15^{+0.46}_{-0.64}$ | $-1.35^{+0.79}_{-0.9}$ |
| Ln C RV [d] | 3,4,5,6 | $\mathcal{U}$ (-10 , 10) | $-5.5^{+3.2}_{-3.0}$ | | | |
| Ln C Phot [d] | 2 | $\mathcal{U}$ (-10 , 10) | $-5.5^{+2.5}_{-2.8}$ | | | |
| Ln $\omega$ RV | 3,4,5,6 | $\mathcal{U}$ (-10 , 10) | | | $-1.21^{+0.08}_{-0.08}$ | |
| Ln $\omega$ Phot | 2 | $\mathcal{U}$ (-10 , 10) | | | $-0.34^{+0.17}_{-0.16}$ | |
| Phase Rot | 3,4,5,6 | $\mathcal{U}$ (0 , 1) | | | | $0.58^{+0.25}_{-0.31}$ |
| C1 [m·ppm$^{-1}$] | | $\mathcal{N}$(0,100) | | | | $-153.29^{+22.93}_{-23.07}$ |
| C2 [m$^2$·ppm$^{-2}$] | | $\mathcal{N}$(0,100) | | | | $8.68^{+13.36}_{-13.57}$ |
| C3 [m$^3$·ppm$^{-3}$] | | $\mathcal{N}$(0,100) | | | | $-9.8^{+7.48}_{-7.63}$ |
| *Instrumental* | | | | | | |
| $F0_{K2}$ [ppt] | 1 | $\mathcal{N}$ (0 , 30) | $0.01^{+0.25}_{-0.25}$ | $0.02^{+0.24}_{-0.24}$ | $0.01^{+0.26}_{-0.26}$ | $-0.01^{+0.51}_{-0.5}$ |
| $F0_{LCO}$ [ppt] | 1 | $\mathcal{N}$ (0 , 30) | $2.4^{+7.4}_{-8.1}$ | $1.74^{+0.59}_{-0.56}$ | $4^{+14}_{-13}$ | |

*Continued on next page*

Table 3 – *Continued from previous page*

| | | | | | | |
|---|---|---|---|---|---|---|
| V0$_{HARPS-N}$ RV [m·s$^{-1}$] | 3 | $\mathcal{N}$ (0 , 100) | $12^{+77}_{-82}$ | -40.1$^{+5.9}_{-6.3}$ | -53$^{+53}_{-53}$ | -54$^{+25}_{-24}$ |
| V0$_{CARMENES}$ RV [m·s$^{-1}$] | 4 | $\mathcal{N}$ (0 , 100) | -34$^{+92}_{-83}$ | $5^{+12}_{-13}$ | -44$^{+73}_{-74}$ | -6$^{+35}_{-37}$ |
| V0$_{SES}$ RV [m·s$^{-1}$] | 5 | $\mathcal{N}$ (0 , 100) | -2$^{+68}_{-84}$ | $0^{+18}_{-17}$ | -52$^{+94}_{-94}$ | -11$^{+39}_{-34}$ |
| V0$_{HERMES}$ RV [m·s$^{-1}$] | 6 | $\mathcal{N}$ (0 , 100) | -16$^{+75}_{-79}$ | -49$^{+16}_{-17}$ | -85$^{+136}_{-137}$ | -39$^{+38}_{-44}$ |
| | | | | | | |
| Ln Jit$_{LCO}$ Flux [ppt] | 2 | $\mathcal{U}$ (-10 , 10) | $1.2^{+0.13}_{-0.15}$ | $1.54^{+0.35}_{-0.27}$ | $1.579^{+0.075}_{-0.075}$ | |
| Ln Jit$_{HARPS-N}$ RV [m·s$^{-1}$] | 3 | $\mathcal{U}$ (-10 , 10) | $3.05^{+0.17}_{-0.18}$ | $3.56^{+0.22}_{-0.29}$ | $2.75^{+0.17}_{-0.19}$ | $4.45^{+0.14}_{-0.14}$ |
| Ln Jit$_{CARMENES}$ RV [m·s$^{-1}$] | 4 | $\mathcal{U}$ (-10 , 10) | -4.9$^{+5.4}_{-3.7}$ | $2.6^{+1.8}_{-7.2}$ | -5.3$^{+4.4}_{-3.1}$ | $4.8^{+0.3}_{-0.2}$ |
| Ln Jit$_{SES}$ RV [m·s$^{-1}$] | 5 | $\mathcal{U}$ (-10 , 10) | -4.7$^{+5.1}_{-3.7}$ | -1.8$^{+4.6}_{-5.3}$ | -3.5$^{+4.6}_{-4.1}$ | $4.3^{+0.6}_{-2.8}$ |
| Ln Jit$_{HERMES}$ RV [m·s$^{-1}$] | 6 | $\mathcal{U}$ (-10 , 10) | -0.3$^{+4.1}_{-6.6}$ | $0.5^{+3.3}_{-6.2}$ | -5.4$^{+5.2}_{-3.2}$ | $4.8^{+0.3}_{-0.3}$ |
| | | | | | | |
| *Limg Darkening* | | | | | | |
| Limb$_L$ | 1 | $\mathcal{U}$ (0 , 1) | $0.26^{+0.16}_{-0.15}$ | $0.36^{+0.16}_{-0.15}$ | $0.42^{+0.12}_{-0.14}$ | $0.44^{+0.17}_{-0.16}$ |
| Limb$_Q$ | 1 | $\mathcal{U}$ (0 , 1) | $0.67^{+0.19}_{-0.25}$ | $0.58^{+0.26}_{-0.33}$ | $0.23^{+0.24}_{-0.16}$ | $0.36^{+0.26}_{-0.21}$ |
| | | | | | | |
| *Residuals* | | | | | | |
| RMS O - C [m s$^{-1}$] | 3,4,5,6 | | 45 | 66 | 48 | 98 |
| RMS O - C [m s$^{-1}$] | 3,4 | | 26 | 14 | 18 | 65 |
| | | | | | | |
| *Bayesian Evidence* | | | | | | |
| Ln$Z$ | | | – 4472 | – 4549 | – 4563 | –3488[1] |

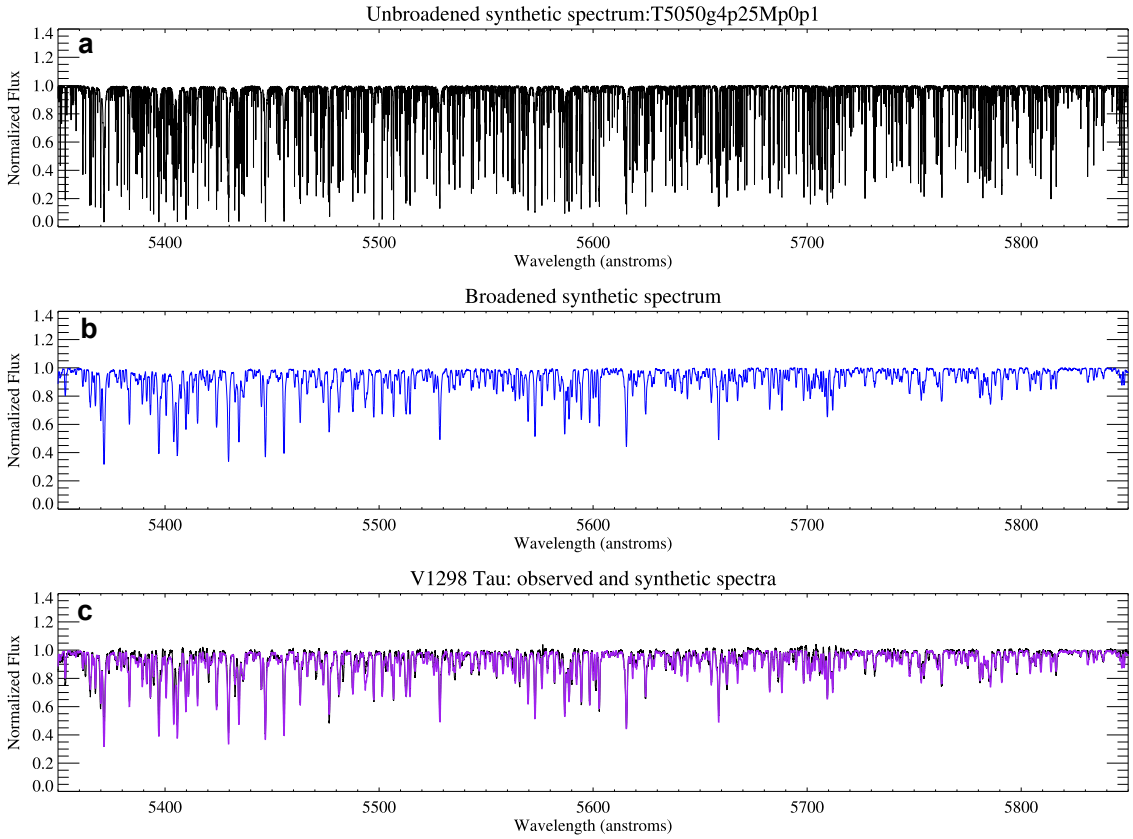


Figure 4: **Best synthetic spectral fit of the HARPS-N spectrum of V1298 Tau.** The interpolated SYNPLE synthetic spectrum without rotational broadening computed for the derived best-fit stellar parameters and metallicity (a), the broadened spectrum with a rotational velocity of 24 $\mathrm{km\,s^{-1}}$ (b) and the observed HARPS-N 1D spectrum of V1298 Tau (black line) together with the best-fit synthetic spectrum (purple line) are displayed in the spectral range 5350–5850 Å (c).

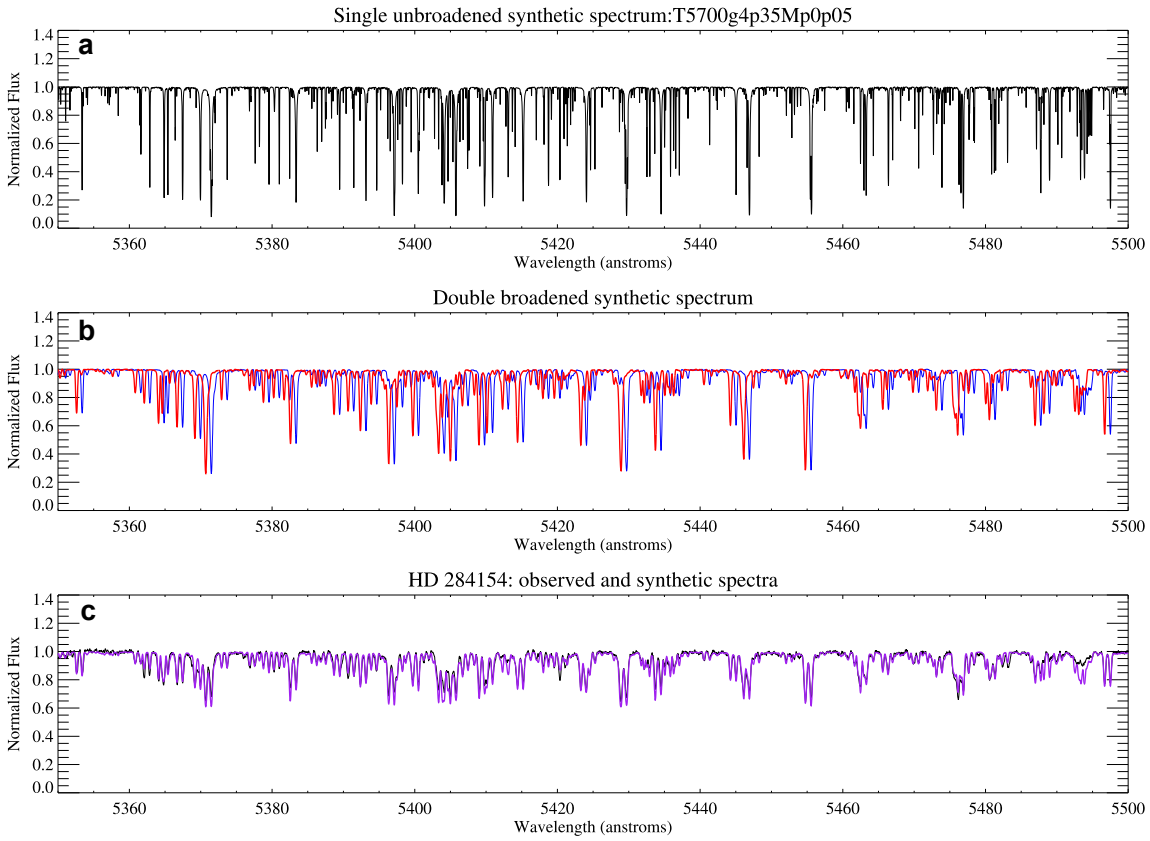


Figure 5: **Best synthetic spectral fit to the NOT FIES spectrum of HD 284154.** The interpolated SYNPLE synthetic spectra without broadening computed for the derived best-fit stellar parameters and metallicity (a), the synthetic spectra separated by RV $\sim 43.6$ km s$^{-1}$ with a rotational velocity of 10 km s$^{-1}$ (b) and the observed FIES 1D spectrum of HD 284154 (black line) together with the best-fit synthetic double-lined spectrum (purple line) are displayed in the spectral range 5350–5850 Å (c).

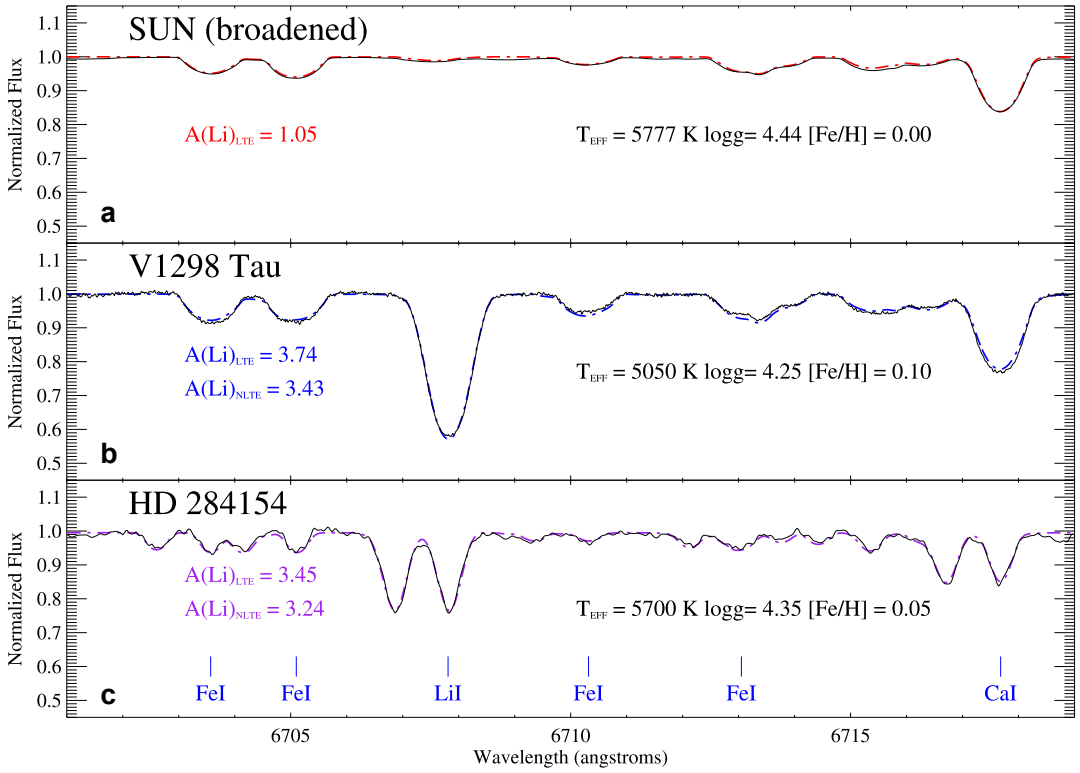


Figure 6: **The lithium spectral region of V1298 Tau and HD 284154.** Spectral region of the lithium doublet around 6708 Å of the solar ATLAS spectrum broadened with a rotation profile of 24 $\mathrm{km\,s^{-1}}$ (a), the HARPS-N spectrum of V1298 Tau (b), and the FIES spectrum of the double-lined spectroscopic binary HD 284154 (c), together with the best-fit MOOG synthetic spectra.

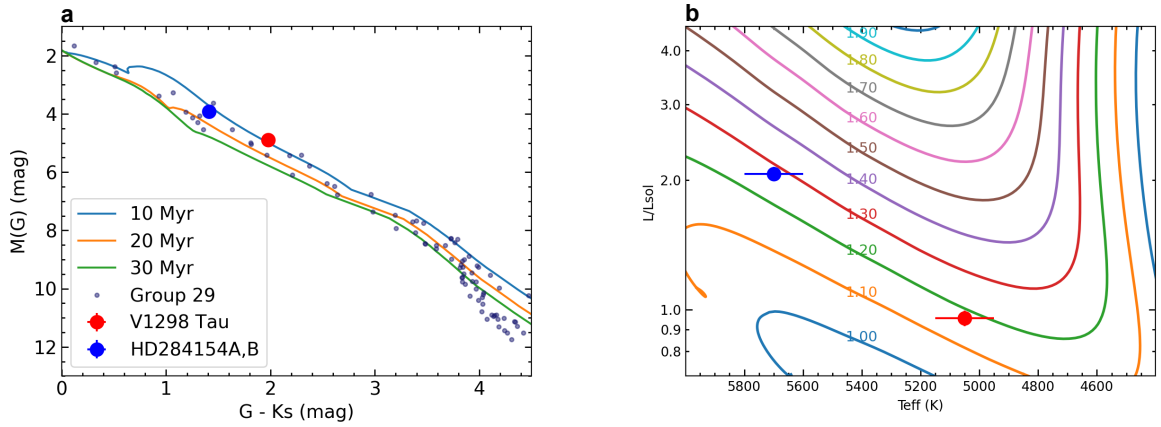


Figure 7: **Position of V1298 Tau and HD 284154 in the colour-magnitude and Hertzsprung-Russel diagrams.** *a:* Colour-magnitude diagram of V1298 Tau and HD 284154A and B (separate components) and the other group 29 members along with various PARSEC isochrones.[67] The 20-Myr isochrone nicely reproduces the sequence of stars with colours $G - K_s < 3.5$ mag while the 10- and 30-Myr isochrones provide acceptable upper and lower envelopes to the observed dispersion of the Group 29 sequence. *b:* Location of V1298 Tau (red) and HD 284154 (blue) in the Hertzsprung-Russel diagram. HD 284154 is decomposed into two equal mass and equal luminosity stars. The tracks for masses between 1.0 and 1.9 $M_\odot$ are also shown and are labeled with the mass value in solar units. Note that the luminosity axis is in logarithmic scale. The error bar in luminosity is of the size of the symbol.